Simultaneous Falsification of ΛCDM and Quintessence with Massive, Distant Clusters

Michael J. Mortonson,[1] Wayne Hu,[2] and Dragan Huterer[3]

[1]*Center for Cosmology and AstroParticle Physics,*
The Ohio State University, Columbus, OH 43210
[2]*Kavli Institute for Cosmological Physics, Department of Astronomy & Astrophysics,*
and Enrico Fermi Institute, University of Chicago, Chicago, IL 60637
[3]*Department of Physics, University of Michigan, 450 Church St, Ann Arbor, MI 48109-1040*

Observation of even a single massive cluster, especially at high redshift, can falsify the standard cosmological framework consisting of a cosmological constant and cold dark matter (ΛCDM) with Gaussian initial conditions by exposing an inconsistency between the well-measured expansion history and the growth of structure it predicts. Through a likelihood analysis of current cosmological data that constrain the expansion history, we show that the ΛCDM upper limits on the expected number of massive, distant clusters are nearly identical to limits predicted by *all* quintessence models where dark energy is a minimally coupled scalar field with a canonical kinetic term. We provide convenient fitting formulas for the confidence level at which the observation of a cluster of mass M at redshift z can falsify ΛCDM and quintessence given cosmological parameter uncertainties and sample variance, as well as for the expected number of such clusters in the light cone and the Eddington bias factor that must be applied to observed masses. By our conservative confidence criteria, which equivalently require masses 3 times larger than typically expected in surveys of a few hundred square degrees, none of the presently known clusters falsify these models. Various systematic errors, including uncertainties in the form of the mass function and differences between supernova light curve fitters, typically shift the exclusion curves by less than 10% in mass, making current statistical and systematic uncertainties in cluster mass determination the most critical factor in assessing falsification of ΛCDM and quintessence.

I. INTRODUCTION

It is well known that the presence of even a single high redshift cluster with sufficient mass can falsify the standard cosmological model where such objects grow from Gaussian initial conditions under the gravitational instability of cold dark matter in a cosmological constant dominated universe (ΛCDM) [1–5]. Robust upper bounds on the number of high mass clusters in ΛCDM arise from the exponential suppression of the dark matter halo number density with mass and the fact that, in the ΛCDM paradigm, geometric constraints on the expansion history determine the growth of structure. Indeed, recently detected massive clusters at high redshift [6–8] have led to claims of tension with ΛCDM [5, 9–11].

More generally, for any given paradigm for dark energy, geometric constraints in combination with CMB constraints on the initial amplitude of fluctuations can be translated into upper bounds on the abundance of high mass clusters. Observational violation of these upper bounds would therefore falsify *all* models of that given paradigm. In particular, in previous work [12] we established that the linear growth function of all quintessence models, where dark energy is a canonical, minimally coupled scalar field, is bounded above to be within a few percent of the ΛCDM values. Here we translate these upper bounds on the linear growth rate to upper bounds on the number of clusters above a given mass and redshift. In particular, we make a conservative assessment of the limiting mass and redshift of a cluster that would rule out all quintessence models that is robust to our present knowledge of cosmological parameters, supernova light

curve fitters, sample variance, and simulation-based calibration of the cluster abundance.

The predictions we present here incorporate cosmological constraints from several recent data sets. In addition to placing limits on the expansion history of the universe, these data also provide important information about the amplitude of matter density fluctuations which directly feeds into cluster predictions. In particular, observations of cosmic microwave background (CMB) anisotropy constrain the amplitude of perturbations at the epoch of last scattering, $z = 1090$. In contrast to many previous studies of the effects of dark energy on the growth of structure, we do *not* take this constraint on the density fluctuations at early times to mean that the amplitude of perturbations at $z = 0$, often characterized by the parameter σ_8, is also well constrained. Instead, we combine CMB constraints with the linear growth functions of quintessence models to set σ_8 so that these models are fully consistent with present CMB data.

We begin in §II by developing methodology to extract cluster abundance probability distributions from expansion history measurements in the context of a given dark energy paradigm. In §III we show how to convert these distributions into confidence levels at which a cluster of a given mass and redshift excludes ΛCDM and quintessence. We consider statistical errors due to parameter and sample variance as well as systematic shifts from uncertainties in observational mass determination, the form of the mass function, and the analysis of supernova data. We discuss these results in §IV.

In Appendix A we provide convenient fitting functions for the relationships between cluster masses, redshifts,

numbers, and confidence levels, as well as the slope of the mass function for bias corrections. In Appendix B we discuss the impact of the CMB normalization of structure, especially in the context of early dark energy. Finally, in Appendix C we discuss two different types of biases induced by measuring observable proxies for mass in the presence of a steep mass function.

II.   METHODOLOGY

Following Refs. [12, 13], we use current constraints on the expansion history of the Universe to make falsifiable predictions for observables related to the growth of structure under specific dark energy paradigms. Here we briefly summarize this technique and highlight changes in the methodology that enable us to obtain robust predictions for the cluster abundance. We begin with descriptions of the data sets we use to constrain the expansion history and the initial amplitude of density fluctuations (§II A), followed by a summary of the likelihood analysis that determines which models in the ΛCDM and quintessence paradigms satisfy the observational constraints (§II B). Finally, we show how we use the output of this analysis to compute probabilities for the abundance of massive, distant clusters in the context of various dark energy paradigms (§II C).

A.   Data Sets

The main observational constraints that inform our predictions for cluster abundances are relative distance measures from Type Ia supernovae (SNe), the CMB temperature and polarization power spectra, baryon acoustic oscillation (BAO) distance measures, and local distance measures of the Hubble constant (H_0).

The Type Ia SN sample we use is the compilation of 288 SNe from Ref. [14], consisting of data from the first season of the Sloan Digital Sky Survey-II (SDSS-II) Supernova Survey, the ESSENCE survey [15], the Supernova Legacy Survey [16], Hubble Space Telescope SN observations [17], and a collection of nearby SN data [18]. The light curves of these SNe have been uniformly analyzed by [14] using both the MLCS2k2 [18] and SALT2 [19] methods. We use the MLCS2k2-analyzed data for most of our results since it leads to the more conservative bound on massive clusters. For example, for flat ΛCDM using MLCS2k2 SN data increases $\sigma_8 \Omega_{\mathrm{m}}^{0.5}$ by $\sim 7\%$ relative to SALT2. In § III C we address the impact of the choice of SN analysis method and also compare with constraints from the Union2 compilation [20] of 557 SNe, which includes the CfA3 sample [21] and a number of SN data sets previously combined in the first Union compilation [22].

For the CMB, we use the most recent, 7-year release of data from the WMAP satellite (WMAP7) [23] employing a modified version of the likelihood code available at the LAMBDA web site [24] which is substantially faster than the standard version while remaining sufficiently accurate [25, 26]. We compute the CMB angular power spectra using the code CAMB [27, 28] modified with the parametrized post-Friedmann (PPF) dark energy module [29, 30] to include models with general dark energy equation of state evolution where $w(z)$ may cross $w = -1$.

We use the BAO constraints from Ref. [31], which combines data from SDSS and the 2-degree Field Galaxy Redshift Survey that determine the ratio of the sound horizon at last scattering to the quantity $D_V(z) \equiv [zD^2(z)/H(z)]^{1/3}$ at redshifts $z = 0.2$ and $z = 0.35$. Since these constraints actually come from galaxies spread over a range of redshifts, and our most general dark energy model classes allow the possibility of significant variations in $H(z)$ and $D(z)$ across this range, we implement the constraints by taking the volume average of D_V over $0.1 < z < 0.26$ (for $z = 0.2$) and $0.2 < z < 0.45$ (for $z = 0.35$). The effect of this volume averaging on the final combined constraints from current data is relatively small.

Finally, we include the recent Hubble constant measurement from the SHOES team [32], based on SN distances at $0.023 < z < 0.1$ that are linked to a maser-determined absolute distance using Cepheids observed in both the maser galaxy and nearby galaxies hosting Type Ia SNe. The SHOES measurement determines the absolute distance to a mean SN redshift of $z = 0.04$ which we implement as $D(z = 0.04) = 0.04c/(74.2 \pm 3.6 \text{ km s}^{-1} \text{ Mpc}^{-1})$.

B.   MCMC Analysis

To predict the cluster abundance using constraints from current data, we use a Markov Chain Monte Carlo (MCMC) likelihood analysis. We take a set of parameters $\boldsymbol{\theta}$ that completely describes a given dark energy class and use a modified version of the code CosmoMC [33, 34] to sample from the joint posterior distribution of the parameters,

$$\mathcal{P}(\boldsymbol{\theta}|\mathbf{x}) = \frac{\mathcal{L}(\mathbf{x}|\boldsymbol{\theta})\mathcal{P}(\boldsymbol{\theta})}{\int d\boldsymbol{\theta} \ \mathcal{L}(\mathbf{x}|\boldsymbol{\theta})\mathcal{P}(\boldsymbol{\theta})}, \qquad (1)$$

where $\mathcal{L}(\mathbf{x}|\boldsymbol{\theta})$ is the likelihood of the data $\mathbf{x}$ given the model parameters $\boldsymbol{\theta}$ and $\mathcal{P}(\boldsymbol{\theta})$ is the prior probability density. We test convergence of the samples to a stationary distribution by applying a conservative Gelman-Rubin criterion [35] of $R - 1 \lesssim 0.01$ across a minimum of four chains for each model class.

For the ΛCDM class we take the parameters

$$\boldsymbol{\theta}_\Lambda = \{\Omega_{\mathrm{m}}, \Omega_{\mathrm{K}}, \Omega_{\mathrm{m}}h^2, \Omega_{\mathrm{b}}h^2, n_s, \ln A_s, \tau\} . \qquad (2)$$

We will mainly consider the flat ΛCDM class here where $\Omega_{\mathrm{K}} = 0$. Additional parameters such as H_0 and Ω_{DE} are derived from this fundamental set. In particular, the

present amplitude of the linear power spectrum σ_8 is a derived parameter (see Appendix B). Our normalization parameter is A_s, the amplitude of the *initial* curvature power spectrum at $k = 0.05\,\mathrm{Mpc}^{-1}$. For all parameters in Eq. (2) we take flat priors that are wide enough that they do not limit the MCMC constraints from current data.

For quintessence we extend the parameter set of Eq. (2) by taking a principal component (PC) decomposition of the dark energy equation of state for $z < 1.7$,

$$w(z) + 1 = \sum_{i=1}^{N_{\max}} \alpha_i e_i(z) \,, \tag{3}$$

where α_i are the PC amplitudes, $N_{\max} = 10$ is the number of components required to form a complete basis with respect to growth and distance measures [12]. These principal components are constructed from the eigenvectors of a projection for the Planck CMB and Super-Nova Acceleration Probe SN covariance matrix for $w(z)$ in sufficiently fine redshift bins to approximate continuous equation of state variations, as described in detail in Ref. [13].

We parametrize the dark energy equation of state at $z > 1.7$ by a constant,

$$w(z > 1.7) = w_\infty \,. \tag{4}$$

While this parametrization does not completely describe all possible behaviors for the equation of state, it does allow for dark energy that is a non-negligible fraction of the total at high redshift or "early dark energy" (EDE). For more restricted model classes without EDE, we fix $w_\infty = -1$ since a constant dark energy density rapidly becomes negligible relative to the matter density at increasing redshift.

In summary, our quintessence parameters are

$$\boldsymbol{\theta}_{\mathrm{Q}} = \{\boldsymbol{\theta}_\Lambda, \alpha_1, \ldots, \alpha_{10}, w_\infty\} \,. \tag{5}$$

Note that flat ΛCDM is a special case of quintessence with $\{\alpha_i, 1 + w_\infty, \Omega_{\mathrm{K}}\} = 0$. We also consider a restricted quintessence class of models which are flat and do not have significant EDE, corresponding to $\{1 + w_\infty, \Omega_{\mathrm{K}}\} = 0$. Quintessence models describe dark energy as a scalar field with kinetic and potential contributions to energy and pressure. Barring models where large kinetic and (negative) potential contributions cancel (e.g. [36]), quintessence equations of state are restricted to $-1 \leq w(z) \leq 1$. Following [13], this bound is conservatively implemented with independent top-hat priors on the PC amplitudes α_i. Any combination of PC amplitudes that is rejected by these priors must arise from an equation of state that violates the bound on $w(z)$, but not all models that are allowed by the priors strictly satisfy this bound. This prior is thus appropriate for making conservative statements on the falsifiability of quintessence. For EDE, quintessence requires $w_\infty \geq -1$, and we additionally impose $w_\infty \leq 0$ to maintain the usual

matter and radiation dominated epochs at high redshift. We adopt a flat prior on $\exp(w_\infty)$ which gives greater weight to models with w_∞ near 0.

C. Cluster Abundance

As described in [13], the MCMC approach allows us to straightforwardly calculate confidence regions for observable quantities determined by the evolution of large-scale structure. The first step is to compute the posterior probability of the linear growth function $G(z)$ from the joint posterior of the dark energy parameters. Note that the growth function we use here scales out the growth of density perturbations during matter domination, $\delta \propto a$, so $G(z) \propto (1+z)\delta$ with normalization $G(z = 10^3) = 1$.

Given the predicted growth function, we compute the abundance of clusters by integrating the product of the halo mass function $dn/d\ln M$ and the comoving volume element over cluster mass and redshift. Since we are interested in the most massive and most distant clusters, we integrate above thresholds in mass and redshift to obtain the expected number of clusters in the full sky with mass $> M$ and redshift $> z$,

$$\bar{N}(M, z) = \int_z^\infty dz' \frac{4\pi D^2(z')}{H(z')} \int_M^\infty \frac{dM'}{M'} \frac{dn}{d\ln M}(M', z') \,, \tag{6}$$

where $4\pi D^2/H$ is the comoving volume element for the full sky written in terms of the comoving angular diameter distance $D(z)$ and the Hubble expansion rate $H(z)$. Note that since the high mass, high redshift mass function falls off rapidly with increasing mass and redshift, $\bar{N}(M, z)$ is typically dominated by the abundance near the threshold values of M and z.

The form of the mass function can be inferred by fitting to the abundance of dark matter halos identified in numerical simulations. The cosmological dependence of the mass function is typically expressed as

$$\frac{dn}{d\ln M} = \frac{\rho_{\mathrm{m},0}}{M} \left| \frac{d\ln\sigma}{d\ln M} \right| f(\sigma, z) \,, \tag{7}$$

where $\sigma(M, z)$ is the rms of linear density fluctuations smoothed over spheres of comoving radius $R = (3M/4\pi\rho_{\mathrm{m},0})^{1/3}$ and $\rho_{\mathrm{m},0} = 3\Omega_{\mathrm{m}} H_0^2/(8\pi G)$ is the present matter density. Here $f(\sigma, z)$ is a function determined by the fit to simulations that depends primarily on $\sigma(M, z)$, but is also weakly dependent on redshift [37, 38].

We study the dependence of our predictions on the specific choice of mass function and describe those tests in the next section, but for definiteness we adopt the Tinker et al. [37] mass function for our main results,

$$f(\sigma, z) = A \left[\left(\frac{\sigma}{b} \right)^{-a} + 1 \right] e^{-c/\sigma^2} \,, \tag{8}$$

with $A = 0.186(1+z)^{-0.14}$, $a = 1.47(1+z)^{-0.06}$, $b = 2.57(1+z)^{-0.011}$, $c = 1.19$. This fit assumes $M = M_{200}$,

defined as the mass within a spherical region around the halo center enclosing an average density equal to 200 times the mean matter density, $\rho_{\mathrm{m},0}(1+z)^3$. We do not adjust the fit parameters for variations in the dark energy model but do test the sensitivity to the fidelity of the fit in §III C.

For the dark energy models and range of scales and redshift that we consider here, the linear growth function is approximately scale-independent, so we can separate the mass and redshift dependence of the density fluctuation rms as

$$\sigma(M,z) = \sigma(M,0) \frac{G(z)}{(1+z)G(0)} \,. \qquad (9)$$

We obtain $\sigma(M,0)$ for each cosmological model using the modified version of CAMB, and compute $G(z)$ by integrating the differential equation for the linear growth function as described in [13]. By using the growth function only to scale backwards from the present epoch, this method includes all high redshift modifications to the transfer function and the CMB normalization of $\sigma(M,0)$ through A_s. We only assume that at the low redshifts of interest $0 < z < 2$ the growth function is independent of scale (see Appendix B for discussion of EDE clustering at early times).

III. CLUSTER PREDICTIONS

From the complete parametrization of the ΛCDM and quintessence model classes and the MCMC posterior probability of the mean number of clusters $\bar{N}$ across the full sky above a given mass and redshift, we can assess the confidence with which the observation of a cluster with that mass and redshift can falsify the model class. We first consider the impact of parameter and statistical uncertainties on the predicted number of massive, high redshift clusters in §III A. In §III B we combine these into exclusion curves in mass and redshift and evaluate the significance of the most massive clusters in the present high redshift sample. Finally, in §III C we illustrate how various systematic errors would shift the upper limits on massive cluster abundances.

A. Parameter and Sample Confidence

We quantify two types of confidence limits for statistical uncertainties. The first is associated with parameter uncertainties on the mean number $\bar{N}$ within the dark energy model class. We call this *parameter variance* and take the one-tailed $100p\%$ confidence level (CL) upper limits on the mean number, $\bar{N}_{Pp}(M,z)$; for example, given the CMB, SN, BAO, and H_0 constraints, there is a 95% probability that the mean number of clusters $> M$ and $> z$ in the full sky is less than $\bar{N}_{P.95}$. To a good approximation, the parameter variance in our cluster abundance predictions corresponds to variance in $\sigma(M,z)$ or,

in particular, σ_8. For example, flat ΛCDM models at the 95% parameter CL have a larger amplitude of fluctuations, $\sigma_8 \approx 0.87$, than the median models with $\sigma_8 \approx 0.83$.

The second confidence limit we define is associated with *sample variance*, under the assumption that the number of clusters in the sample is Poisson distributed with mean $\bar{N}$ across the full sky. This assumption ignores the clustering of clusters and should be a good approximation in the rare object limit [39]. In particular, the probability to have zero clusters in a random sample of a fraction of sky f_{sky} is $s \equiv e^{-\bar{N}f_{\mathrm{sky}}}$. We therefore define the sample variance $100s\%$ CL for models with a mean number of clusters in the *full sky* as

$$\bar{N}_{Ss}(f_{\mathrm{sky}}) \equiv -f_{\mathrm{sky}}^{-1} \ln s \,. \qquad (10)$$

That is, if the mean number of clusters above M and z expected in the full sky is $\bar{N}_{Ss}$ for a particular model, then that model would be excluded at the $100s\%$ CL by one or more such observed clusters in a survey covering f_{sky} of the full sky. For example, the observation of one or more clusters at redshift z with mass M observed in $300\,\mathrm{deg}^2$ ($f_{\mathrm{sky}} \approx 0.0073$) would exclude models that predict a mean number of clusters in the full sky $\bar{N}(M,z)$ less than $\bar{N}_{S.95} \approx 7.1$ at the 95% sample CL.

Some care must be taken to define the appropriate f_{sky} for a given cluster. For example, if out of many similar surveys only one reported a high mass cluster, then the appropriate sky area is the total area of the surveys, not just the individual survey area selected to have the cluster *a posteriori*. The most conservative limits are obtained by taking $f_{\mathrm{sky}} = 1$ when interpreting any observation, i.e. assuming that all unobserved regions of the sky do not host clusters with anomalously high masses and redshifts. In this case $\bar{N}_{S.95} \approx 0.051$. Compared with, say, the median prediction $\bar{N}_{S.50} = 95$ at $300\,\mathrm{deg}^2$, these criteria are a factor of ~ 1900 more conservative in predicted number.

We combine these two types of uncertainties to compute the maximum cluster mass and redshift within some area of the sky predicted by a particular model class. The mass and redshift limits corresponding to $100s\%$ sample CL and $100p\%$ parameter CL can be found by taking $\bar{N}_{Ss}(f_{\mathrm{sky}}) = \bar{N}_{Pp}(M,z)$ to get

$$\int_{-\infty}^{\log(-f_{\mathrm{sky}}^{-1} \ln s)} d\log \bar{N} \, P(\log \bar{N}|M,z) = p \,, \qquad (11)$$

where $P(\log \bar{N}|M,z)$ is the posterior density in the expected number of clusters above M and z for the given class of dark energy models. For simplicity, we will often consider the case $s = p$ and refer to this as the "$100s\%$ joint CL" for sample and parameter variance. Note that in this approach observational uncertainty in determining the mass, which varies from cluster to cluster, is not directly included so that the cluster mass errors must be included when comparing with the $M(z)$ exclusion curves presented in §III B (see also Appendix C).

Finally, one can also test whether the N rarest clusters together place a substantially stronger bound on the dark energy paradigm than the single rarest object detected so far. To do this, one computes the Poisson probability using the mass and redshift threshold that includes all of those N clusters. For example, for the two rarest clusters the mean number $\bar{N}_{Ss}^{(2)}$ corresponding to exclusion at the $100s\%$ sample CL can be found from

$$s = \left(1 + f_{\rm sky} \bar{N}_{Ss}^{(2)}\right) e^{-f_{\rm sky} \bar{N}_{Ss}^{(2)}} \qquad (12)$$

to be

$$\bar{N}_{Ss}^{(2)} = -f_{\rm sky}^{-1}[1 + W_{-1}(s)], \qquad (13)$$

where W_{-1} is the lower branch of the Lambert W function. If $f_{\rm sky}\bar{N}_{Ss}^{(2)} \ll 1$, $\bar{N}_{Ss}^{(2)} \approx f_{\rm sky}^{-1}\sqrt{2(1-s)}$. The expected number for the 95% joint CL at $f_{\rm sky} = 1$ is $\bar{N}_{S.95}^{(2)} = 0.355$, compared with $\bar{N}_{S.95} = 0.051$ for the single most extreme cluster; therefore, the model is required to predict a mean abundance 7 times larger to explain two clusters above a given mass and redshift rather than one. This statistic is conservative in the sense that the rarest cluster is typically treated as if it were only as rare as the second rarest cluster (more specifically both clusters are assigned the lowest M, z of the pair). Thus the $N = 2$ test can actually be weaker than the $N = 1$ rarest cluster test. It can be applied sequentially to the N rarest clusters by defining $\bar{N}_{Ss}^{(N)}$ as the solution to

$$s = \sum_{i=0}^{N-1} \frac{(f_{\rm sky}\bar{N}_{Ss}^{(N)})^i}{i!} e^{-f_{\rm sky}\bar{N}_{Ss}^{(N)}}. \qquad (14)$$

Again if $f_{\rm sky}\bar{N}_{Ss}^{(N)} \ll 1$, $\bar{N}_{Ss}^{(N)} \approx f_{\rm sky}^{-1}[N!(1-s)]^{1/N}$. In the confidence level fitting formula of Eq. (A10) one simply replaces

$$-f_{\rm sky}^{-1} \ln s = \bar{N}_{Ss} \to \bar{N}_{Ss}^{(N)}. \qquad (15)$$

Note however that the number of trials taken before finding an anomaly must be considered in interpreting the exclusion.

B. Model Exclusion

We begin with the flat ΛCDM predictions. In Fig. 1 we show the posterior distributions of $\log \bar{N}$ for representative choices of M and z. As either increases, the mean number drops below unity and the observation of even a single cluster at that mass and redshift becomes unlikely. The dotted vertical line represents the 95% sample CL threshold $\bar{N}_{S.95}(f_{\rm sky} = 1)$. When M and z are large enough that 95% of the parameter probability distribution $P(\log \bar{N})$ lies below this line, we consider the flat ΛCDM class ruled out at the 95% joint CL by an observation of even a single cluster of mass M at redshift z.
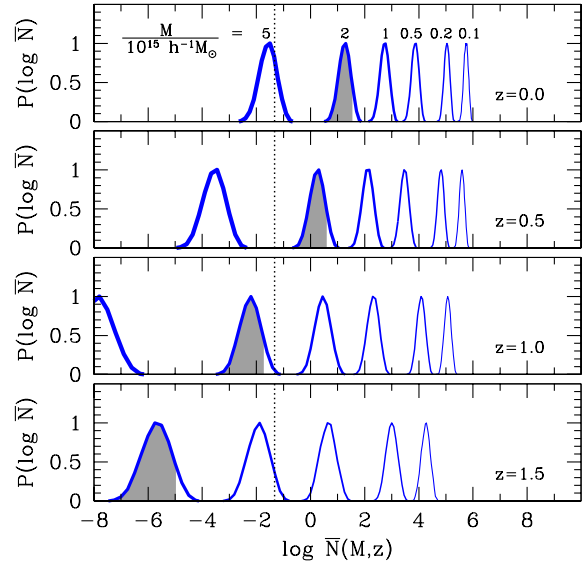

FIG. 1. Predicted mean, full-sky abundance $\bar{N}(M, z)$ of clusters above mass and redshift thresholds M and z, respectively, for flat ΛCDM models that fit current CMB+SN+BAO+H_0 data. Vertical dotted lines are plotted at $\bar{N}_{S.95}(f_{\rm sky} = 1)$, the 95% CL sample variance limit for a full-sky survey. For $M = 2 \times 10^{15}\,h^{-1}\,M_\odot$, we shade the lower 95% of each distribution; exclusion at the 95% *joint* CL for a cluster of this mass in the full sky occurs at the redshift for which all of the shaded area lies to the left of the vertical $\bar{N}_{S.95}(f_{\rm sky} = 1)$ line (in this case, $z \approx 0.9$). Probability distributions here and in later figures are normalized so that $\max[P(\log \bar{N})] = 1$.

In Appendix A, we provide a convenient fitting formula for the dependence of these flat ΛCDM exclusion masses on redshift, $f_{\rm sky}$ and the sample and parameter variance confidence level parameters s and p (see Eq. A9). Figure 2 uses these fitting formulas to illustrate how the sample and parameter variance limits change relative to our default 95% joint CL full sky limit with variations in $f_{\rm sky}$, s, and p.

Next we generalize these results to different dark energy model classes. Figure 3 shows the predictions for $M = 10^{15}\,h^{-1}\,M_\odot$ and $z = 1.48$ which is at the 95% joint CL for flat ΛCDM. With nonzero curvature, the confidence level for this choice of M and z remains nearly unchanged at 93% parameter CL, reflecting the fact that curvature is well constrained in the ΛCDM context. On the other hand, the parameter confidence level at which models are excluded with 95% sample CL actually increases as the model class widens to flat quintessence without EDE (98.8%) and to nonflat quintessence with EDE (99.7%) (see shading in Fig. 3). This is in spite of the fact that flat ΛCDM is included as a special case of each of these classes. In the quintessence classes there are simply more ways of reducing the growth function at the relevant redshifts through parameter variations than increasing it. Hence the low-$\bar{N}$ tail of the distribution is highly dependent on the prior placed on the parameters.
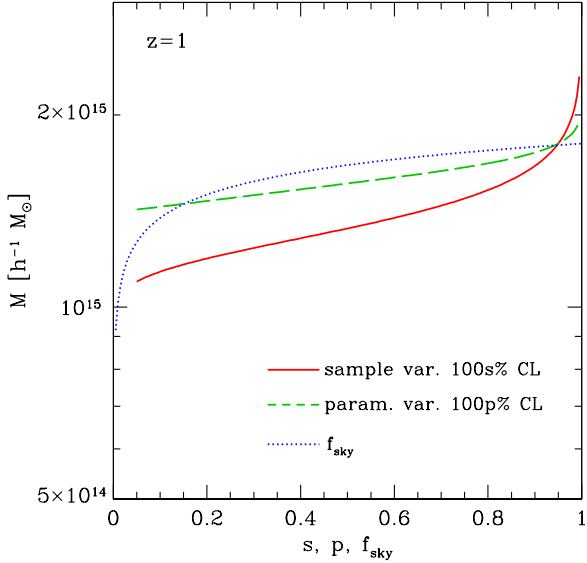
FIG. 2. Dependence of the flat ΛCDM mass threshold at $z = 1$ on sample variance s and parameter variance p confidence levels and on the sky fraction $f_{\rm sky}$. Individual variations are computed using the fitting functions of Appendix A with one parameter varied at a time and the remaining parameters fixed to the fiducial values of $s = 0.95$, $p = 0.95$, and $f_{\rm sky} = 1$.

FIG. 3. Predicted mean, full-sky abundance of clusters with $M > 10^{15} \, h^{-1} \, M_\odot$ and $z > 1.48$, for flat and nonflat ΛCDM, flat quintessence without early dark energy, and nonflat quintessence with early dark energy. The vertical dotted line marks $\bar{N}_{S,95}(f_{\rm sky} = 1)$, i.e. a $10^{15} \, h^{-1} \, M_\odot$ cluster at $z = 1.48$ observed anywhere in the sky would exclude all models in $P(\log \bar{N})$ to the left of the dotted line with a significance of at least 95% sample CL. The lowest-$\bar{N}$ 95% of each distribution is shaded.

One might therefore worry that the exclusion of quintessence models at the high-$\bar{N}$ tail of the distribution might also depend strongly on the prior. Parameter choices in the tail of the distribution would then have likelihoods as good as or better than at the median. This pathology does not occur here. For example, among the 5% of flat ΛCDM models in Fig. 3 with $\bar{N} > 0.051$ the best fit model has a likelihood that is worse than the global maximum likelihood (for all $\bar{N}$) by $-2\Delta \ln \mathcal{L} = 3.3$, consistent with a one-tailed 95% CL. The best fit quintessence model (nonflat, with EDE) with $\bar{N} > 0.051$ fits the data worse than the global maximum likelihood for quintessence by $-2\Delta \ln \mathcal{L} = 7.5$, also consistent with the higher confidence for exclusion of quintessence models.[1]

For values of M and z other than those used in Fig. 3, the dependence of $P(\log \bar{N})$ on the dark energy model class is similar. A massive, high z cluster that convincingly falsified ΛCDM would also falsify *all* quintessence models. This robustness is a consequence of the firm upper limit that flat ΛCDM places on the quintessence growth function noted in [12] and is essentially due to

the quintessence requirement that $w(z) \geq -1$. Hereafter we adopt the parameter confidence level of flat ΛCDM for all quintessence cases to avoid the semantic problem of ruling out quintessence at a higher parameter confidence than ΛCDM even though ΛCDM is a subset of quintessence.

In Fig. 4 we show the 95% joint CL upper limit in the mass-redshift plane for flat ΛCDM. An observation of one or more clusters at M and z that lie anywhere above the limit corresponding to a given $f_{\rm sky}$ would rule out both ΛCDM and quintessence. We further find that the typical realization of the typical ΛCDM model, corresponding to the 50% joint CL, would move the limiting curve down by a factor of approximately 1.6 in mass (for $f_{\rm sky} = 1$). If we keep the 50% joint CL and also reduce $f_{\rm sky}$ to correspond to a 300 deg^2 area, the mass threshold differs from our fiducial $f_{\rm sky} = 1$ and 95% joint CL by a factor of ~ 3.2 in mass. Therefore, to rule out ΛCDM and quintessence by our fiducial criteria, the mass of the cluster must be at least 3.2 times the typical ΛCDM prediction for the largest cluster in a 300 deg^2 survey, and 1.6 times the prediction for the most massive cluster across the whole sky.

With these conservative criteria none of the reported high mass, high z clusters falsify ΛCDM or quintessence. The two that provide the most tension with these model classes are SPT-CL J0546-5345 [8, 40] at $z = 1.07$ which has an X-ray Y_X-determined mass of $M_{200} = (8.23 \pm 1.21) \times 10^{14} \, M_\odot$ and XMMU J2235.3-2557 [6, 9, 41] at

_____

[1] Quintessence models in the tail of the distribution can actually have a better absolute likelihood than ΛCDM models in the tail or even the median ΛCDM model due to the better fit of $w \approx -0.8$ models to the MLCS2k2-analyzed SN data [14], while still being strongly disfavored due to a large amplitude of structure A_s (or σ_8).
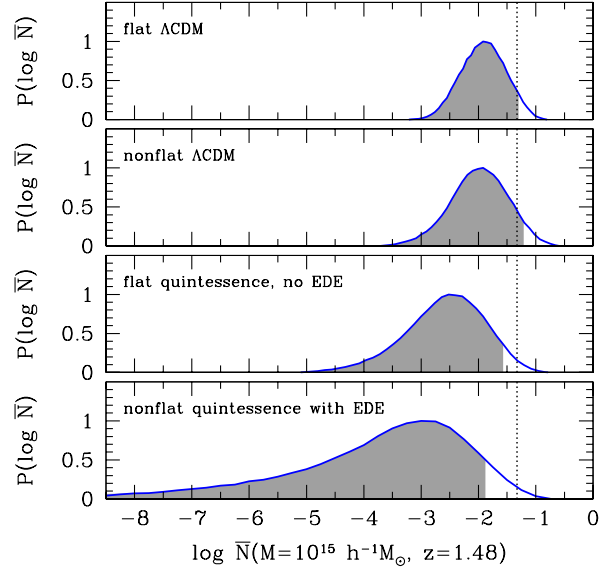
$z = 1.39$ with an X-ray (T_X) mass of $7.7^{+4.4}_{-3.1} \times 10^{14} \, M_\odot$. These X-ray mass estimates are consistent with masses obtained by other means such as weak lensing, and our most conservative conclusions requiring 95% joint CL significance in the full sky would not be greatly changed by using alternate mass proxies.

For a more aggressive interpretation of the data, one can estimate the effective f_{sky} values for these measurements. They are somewhat subjective in that the clusters are the most massive ones found in all high z Sunyaev-Zel'dovich (SZ) and X-ray surveys respectively. The first release of the South Pole Telescope (SPT) SZ cluster survey covered 178 deg², whereas the Atacama Cosmology Telescope SZ survey covered 455 deg² [42] of which ~ 50 deg² overlap with the first-release SPT fields. On the other hand X-ray surveys have covered some 283 deg² for $1.0 < z < 2.2$ [11]. We therefore plot these clusters in Fig. 4 (lower panel) against an exclusion curve for 95% joint CL at 300 deg², using $h = 0.70$ as assumed in Refs. [40, 41] to convert the masses to units of $h^{-1} \, M_\odot$.[2] Note that the $M(z)$ level is only weakly dependent on f_{sky} for order unity rescalings (see Fig. 2).

Even under this more aggressive interpretation of the exclusion limit, these two clusters do not convincingly rule out ΛCDM or quintessence. Although their redshifts and mean masses are somewhat atypical in that they exceed the 50% joint CL exclusion curve, neither cluster is more significant than the 95% joint CL. For example, taking the mean reported masses and fixing the parameter variance confidence level at 95%, SPT-CL J0546-5345 is only at 44% sample CL (using the fitting formula of Appendix A), i.e. it is a typical result for flat ΛCDM. The mean for XMMU J2235.3-2557 yields a higher 89% sample CL, but taking the 1 σ lower limit on the mass brings the confidence all the way down to 8%. Even combining the two using Eq. (12) and a joint sky area of 600 deg² does not improve the confidence. In fact in this conservative test where thresholds are set to the lowest mass and redshift of the pair, the joint sample confidence level using the mean masses actually decreases to 30%.

C. Systematic Shifts

Systematic shifts in the observational mass determination, the theoretical mass function, and SN data analysis techniques can strongly affect the confidence with which ΛCDM and quintessence can be excluded. Here we quantify the impact of each of these systematic effects on the predicted abundance of high mass, high redshift clusters.
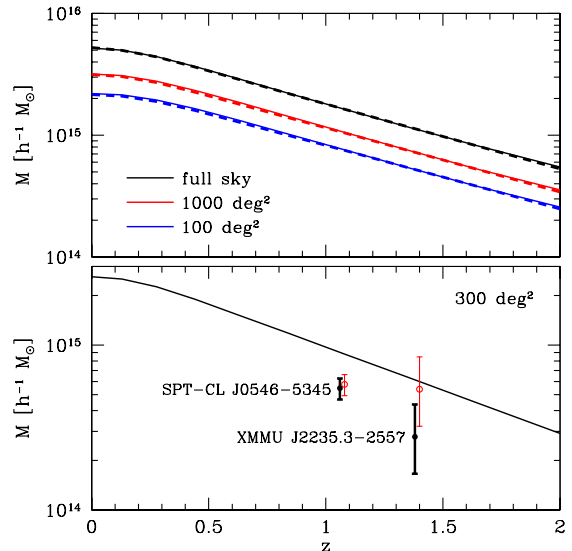

FIG. 4. $M(z)$ exclusion curves. Even a single cluster with (M, z) lying above the relevant curve would rule out both ΛCDM and quintessence. *Upper panel:* flat ΛCDM 95% joint CL for both sample variance and parameter variance for various choices of sky fraction f_{sky} from the MCMC analysis (thin solid curves) and using the fitting formula from Appendix A (thick dashed curves; accurate to $\lesssim 5\%$ in mass). *Lower panel:* Two of the most anomalous clusters detected to date, compared with the 95% joint CL exclusion curve for 300 deg² which approximates the total survey area for each cluster. We show the X-ray determined masses with and without Eddington bias correction (black solid points with thick error bars and red open points with thin error bars, respectively, offset in redshift by ± 0.01 for clarity).

Despite numerous recent advances in mass estimation methods, the determination of cluster masses is still quite uncertain. Different methods do not always yield consistent results, and in some cases the mass may be systematically over- or underestimated. Since cluster abundances fall off exponentially with mass at high masses, even small errors in the estimated masses correspond to large shifts in the expected number of clusters.

In the upper panel of Fig. 5, we show the impact on $\bar{N}$ of changing cluster masses by $\pm 10\%$ or $\pm 30\%$; these offsets are representative of the range in systematic uncertainty in current determinations of cluster masses. Systematic errors in mass are most important for the rarest clusters due to the increasing steepness of the mass function. For $M = 10^{14} \, h^{-1} \, M_\odot$ and $z = 0$, a 30% offset in mass shifts $\bar{N}$ by a factor of ~ 2, but for the $10^{15} \, h^{-1} \, M_\odot$, $z = 1.5$ case shown in Fig. 5 systematic shifts in mass can change the expected abundance by orders of magnitude, making an ordinary cluster appear to be exceedingly unlikely in the context of a given cosmology or vice versa. In the $M(z)$ exclusion plane of Fig. 4, these systematic offsets can be incorporated as simple shifts in the data points.

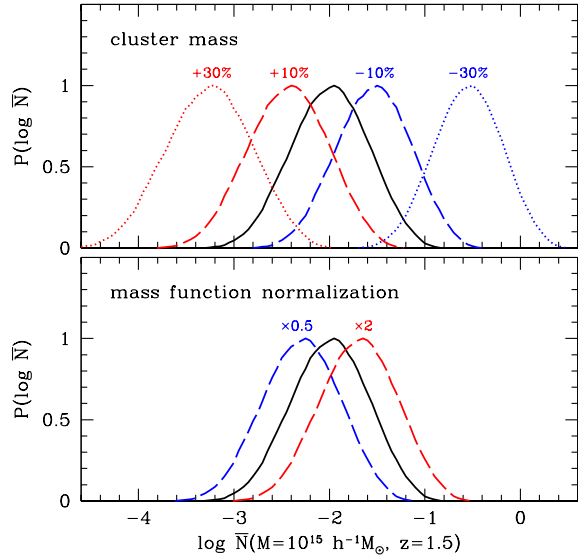Estimation of the rarest cluster masses is also subject

FIG. 5. Impact of systematic errors in cluster mass determination and mass function amplitude on the mean number of clusters in the full sky with $M > 10^{15} \, h^{-1} \, M_\odot$ and $z > 1.5$ for flat ΛCDM. A fractional change in mass determination can change the number of clusters by orders of magnitude. Conversely, a factor of two change in the mass function amplitude near this mass and redshift changes the mass limits by only a few percent.

to Eddington bias, where selection effects shift the determined masses in a manner that depends on the cosmology. If a cluster is selected as anomalous due to the high value of some observable quantity, e.g. X-ray flux and temperature, optical richness, or SZ decrement, the steep mass function makes scattering from low masses to high observables more likely than scattering from high masses to low observables [43]. In Appendix C we discuss two sorts of mass biases associated with this effect that should not be confused. For the purposes of comparing to $M(z)$ exclusion curves and for an observable mass $M_{\rm obs}$ that is lognormally distributed around the true mass, one should correct $M_{\rm obs}$ for bias by [44, 45]

$$\Delta \ln M = \frac{\gamma}{2} \sigma_{\ln M}^2 \, . \qquad (16)$$

Here γ is the local logarithmic slope of the mass function $dn/d\ln M \propto M^\gamma$. In Appendix A we provide an approximate expression for $\gamma(\bar{N}, z)$ in Eq. (A6). Note that for our default 95% joint CL constraint with $\bar{N} = 0.051$ and $z \sim 1$, $\gamma \approx -8$. For $\sigma_{\ln M} = 0.3$ this bias is $\Delta \ln M \approx 0.36$ and can have a substantial impact on the CL level of exclusion should such a high mass cluster ever be found (see Fig. 4). The logarithmic slope is much steeper at this high level of exclusion than the typical expectation for the most massive cluster in 300 deg^2 of $\bar{N} = 95$ where $\gamma \approx -5$ at $z \sim 1$.

Specifically, to correct for Eddington bias in placing an observed cluster whose mass-observable relation implies $\ln M = \ln M_{\rm obs} \pm \sigma_{\ln M}$ on the $M(z)$ exclusion plots,

one does the following. Take the implied γ for the $M_{\rm obs}$, redshift, and parameter confidence level p using Eq. (A8) and Eq. (A6), and evaluate the shift in mass due to number bias using Eq. (16). Then take the mean mass and confidence limits and shift them down by this bias factor. If the cluster still lies in the excluded region of the $M(z)$ plane, then it falsifies ΛCDM and quintessence at the chosen confidence level. This procedure assumes that the mass function slope is approximately the same at $M_{\rm obs}$ as it is for the true cluster mass, which holds as long as the scatter $\sigma_{\ln M}$ is not too large.

In Fig. 4 we show examples of the Eddington bias correction assuming flat ΛCDM for SPT-CL J0546-5345 and XMMU J2235.3-2557 where we take the reported mass errors as a proxy for $\sigma_{\ln M}$. These examples should only be taken as illustrative since not all of the sources of mass error are lognormally distributed or random. Note that the large mass errors for the higher redshift cluster and the steeper slope of the mass function both contribute to a bias that is as large as the statistical errors, although the bias correction from Eq. (16) may be somewhat overestimated given the large $\sigma_{\ln M}$ as noted above. Taking this bias estimate at face value, the sample variance CL is reduced drastically for the corrected mean mass to $< 1\%$ for 95% parameter confidence and 300 deg^2, whereas the significance of the SPT cluster only falls to 33% given its smaller reported mass error. Relative to ΛCDM, quintessence models on average predict that massive, high redshift clusters are rarer, resulting in a steeper logarithmic slope γ and a larger bias correction.

Finally, the mass *definition* used in the theoretical predictions must be chosen to correspond to a quantity that is tightly correlated with the observables and consistent with the simulation-calibrated mass function. In particular, the scatter between halo masses in simulations using spherical overdensity and friends-of-friends halo definitions is large and asymmetric, and the difference in mass definitions for a single halo can be a factor of two or more [37, 46].

Compared with systematic errors in cluster masses, the impact of systematic errors in the amplitude of the mass function near the relevant mass and redshift thresholds is far less severe. In particular, although the effect on the mass function of generalizing to dynamical dark energy models is still largely untested by simulations, even a factor of 2 change in the mass function normalization [i.e. A in Eq. (8)] has less impact than a 10% offset in mass (Fig. 5, lower panel). For reference, neglecting the redshift dependence of the mass function parameters $\{A, a, b\}$ decreases the amplitude by a smaller 40% shift for ΛCDM (equivalent to a 3% mass offset) near $M = 10^{15} \, h^{-1} \, M_\odot$ and $z = 1.5$. Following the suggestion of Ref. [37], we also test the impact of replacing the redshift dependence of the mass function parameters with dependence on the growth function. Specifically, for a redshift threshold z we evaluate the parameters $\{A, a, b\}$ in Eq. (8) at a different redshift $\tilde{z}$ satisfying

$$(1 + \tilde{z})^{-1} G_\Lambda(\tilde{z}) = (1 + z)^{-1} G(z) \, , \qquad (17)$$

8

where $(1+z)^{-1}G_\Lambda(z)$ is the density growth function for a fiducial flat ΛCDM model. This modification has a negligible effect on $P(\log \bar{N})$ and changes the abundance predicted for individual models by $< 10\%$ even in the most general class of nonflat quintessence models with EDE.

Likewise, extrapolation of the mass function to masses and redshifts outside the range calibrated to simulations should have a subdominant effect on the overall systematic errors. For the mass function we use here, the simulations of [37] probe the range $0.4 \lesssim \sigma \lesssim 4$ at $z \lesssim 2$ to better than $\sim 5\%$ accuracy. For the median ΛCDM model, the lower limit of this range corresponds to a maximum mass $M \approx 3.1 \times 10^{15}\,h^{-1}\,M_\odot$ at $z = 0$, and $M \approx 1.0 \times 10^{14}\,h^{-1}\,M_\odot$ at $z = 2$. For the 95% parameter CL ΛCDM models used to construct the exclusion curve in Fig. 4 these masses are slightly higher: $M \approx 3.7 \times 10^{15}\,h^{-1}\,M_\odot$ at $z = 0$ and $M \approx 1.2 \times 10^{14}\,h^{-1}\,M_\odot$ at $z = 2$. Thus at high redshift the 95% joint confidence exclusion curves in Fig. 4 require an extrapolation of up to a factor of ~ 4 in mass for $f_{\mathrm{sky}} = 1$ and a factor of ~ 2 for 300 deg^2. On the other hand, Hubble volume light cone simulations show no strong deviations from this mass function [47] from which one can infer that the scaling holds at least to order unity down to $\bar{N} \sim 1$; this includes the 95% sample CL rarity for survey areas up to ~ 2000 deg^2.

Systematic errors in the data analysis that propagate into the posterior distributions $P(\log \bar{N})$ can also change the confidence at which models can be excluded. The largest systematic effects from these data sets at present appear to come from the analysis of the SN data; in particular, the choice of method for fitting SN light curves (specifically, MLCS2k2 or SALT2) has been shown to affect constraints on a constant dark energy equation of state at the level of $\Delta w \sim 0.2$ [14]. While this specific systematic error will likely be reduced as its causes are better understood (e.g. [48]), we have adopted the MLCS2k2 technique for our main results since it provides the more conservative constraints for assessing exclusion of ΛCDM and quintessence.

Even for flat ΛCDM, the choice of SN methodology affects cluster abundance predictions. Figure 6 (top panel) shows a factor of 2 difference in abundance for $M = 10^{15}\,h^{-1}\,M_\odot$ and $z = 1.5$. The offset between MLCS2k2 and SALT2 varies with the mass and redshift thresholds, but corresponds to an approximately constant shift of 10% in the effective mass threshold for all $z < 2$. In Appendix A we describe how to account for this 10% shift in our fitting formulas. For ΛCDM, this difference is mainly due to the preference for lower Ω_{m} when using the SALT2 light curve fitter in place of the MLCS2k2 method. The lower Ω_{m} also drives down the present day normalization for fixed initial curvature A_s. The best fit values of $(\Omega_{\mathrm{m}}, \sigma_8)$ are $(0.29, 0.83)$ with MLCS2k2 and $(0.27, 0.81)$ with SALT2 (including the CMB, BAO, and H_0 constraints as well as SN data). Using the SALT2 analysis in fact alleviates some tension
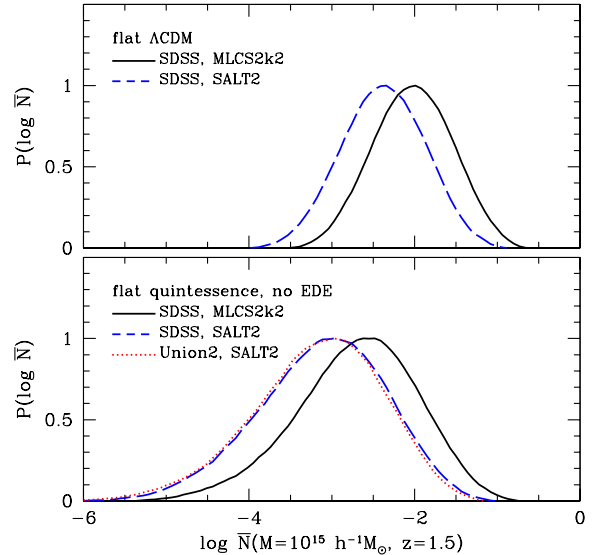

FIG. 6. Effect of SN systematics on $P(\log \bar{N})$ at $M = 10^{15}\,h^{-1}\,M_\odot, z = 1.5$ for flat ΛCDM (top) and flat quintessence without early dark energy (bottom). The choice of light curve fitter when analyzing the SDSS compilation of SN data affects the predicted growth history, which leads to a systematic shift in the predicted cluster abundance. Switching from MLCS2k2 to SALT2 has an effect comparable to increasing the mass threshold by 10% (see Fig. 5). The bottom panel also shows quintessence predictions using the Union2 compilation of SN data, analyzed with the SALT2 method, which are almost identical to the SALT2 predictions with the SDSS SN compilation.

between the CMB and SN data in flat ΛCDM.

The SN distances estimated using the SALT2 method, unlike MLCS2k2, depend on an assumed cosmological model and so compiled data sets analyzed assuming ΛCDM formally should not be applied to quintessence [14]. However it is both instructive and common practice to do so to approximate the impact on dark energy constraints. As in flat ΛCDM, using the SALT2 method for flat quintessence with no EDE on the same data set lowers the predicted number of clusters (see Fig. 6 bottom panel) by a factor of 2 for $M = 10^{15}\,h^{-1}\,M_\odot$ and $z = 1.5$, corresponding to a $\sim 10\%$ shift in mass. However, for quintessence models this offset is due to differences in the preferred dark energy parameters as well as in Ω_{m}. We also show in Fig. 6 the impact of switching the SN data to the Union2 compilation, which also used the SALT2 method [20]. Note that the cluster predictions for the two SALT2 cases are nearly identical, despite using different sets of SNe.

We thus have good evidence that flat ΛCDM exclusion curves with either SN light curve fitter provide the same implications for quintessence. The main difference is a shift in the median ΛCDM prediction. Using the MLCS2k2 light curve fitter predicts higher numbers and hence is more conservative for our exclusion analysis. Translated into masses, the switch to SALT2 corresponds

to a 10% decrease in the mass of the $M(z)$ exclusion limits of Fig. 4. This 10% shift moderately increases the significance of observed clusters. Using the mean X-ray masses without Eddington bias correction, and taking the 95% parameter CL for a 300 deg^2 area, the sample variance significance shifts from 44% to 62% for SPT-CL J0546-5345 and from 89% to 94% for XMMU J2235.3-2557.

IV. DISCUSSION

In this paper we have analyzed predictions for the abundance of massive, distant clusters using an observationally complete basis for the quintessence paradigm. Physically, this paradigm assumes that dark energy is a non-interacting canonical scalar field. Phenomenologically, quintessence is a spatially smooth component of energy density compared with dark matter below the horizon scale with an equation of state $-1 \leq w(z) \leq 1$.

We have shown that any observation that purports to rule out ΛCDM from the existence of massive clusters at any redshift also rules out quintessence, since quintessence models can suppress but not enhance the abundance of rare clusters compared to ΛCDM. This conclusion still holds if dark energy is a non-negligible fraction of the total density at high redshift. Once normalized to the CMB, quintessence models can only reduce the number of clusters (cf. [49–54]).

We have provided convenient fitting functions that can be used to evaluate the confidence level of exclusion of a class of dark energy models due to the observation of a cluster of a given mass at a given redshift. In doing so, we have accounted for two sources of variance: *parameter variance*, that current data allow cosmological parameters to take a range of values, and *sample variance*, the Poisson noise in counting rare objects in a finite volume. Our formulas can also be used to quickly evaluate the expected number of clusters in ΛCDM.

The single most important element of any claim of model exclusion due to observation of a massive, high redshift cluster is the robustness and accuracy of the mass measurement. In particular, it is important to account for Eddington bias, the fact that the steep mass function will cause lower mass objects to scatter into a sample defined by thresholds in observable proxies for mass. We include corrections for Eddington bias in our analysis, and clarify the difference between the two types of mass shifts found in the literature under this name.

When phrased in terms of shifts in the limiting mass, other systematic effects are relatively minor in comparison. For example, order unity variations in the mass function amplitude correspond to $< 10\%$ changes in the exclusion mass. Likewise the difference between predictions from SN data fit with the SALT2 and MLCS2k2 methods, which produces a systematic shift of $\Delta w \sim 0.2$, also corresponds to a 10% effect in mass.

Finally, we have seen that the interpretation of clus-

ter limits depends strongly on the effective survey area in which the clusters were selected, whereas the actual sky area of the data is often much smaller. The most conservative interpretation of the most massive cluster in a survey is that there is at least one such object in the whole sky. Interpreted in this fashion, none of the clusters reported in the literature can be deemed to falsify ΛCDM or quintessence. Even when interpreted at an estimated few hundred square degrees for the effective area, these clusters fail to convincingly falsify either paradigm.

Our results differ qualitatively from those in Refs. [5, 9–11] which claim that the observed massive, high redshift clusters rule out the ΛCDM paradigm at ~ 2–4σ. The different conclusions can be explained by the fact that these works do not undertake a full treatment of parameter variance and do not correct the observed masses for Eddington bias and/or interpret mass measurements to have smaller errors. Moreover, for single cluster analyses Refs. [5, 9, 10] take an inappropriately small effective sky area. For XMMU J2235.3-2557, a shift in the effective sky area from 11 deg^2 to 300 deg^2 alone accounts for a factor of 1.7 in the exclusion mass [11]. On the other hand, we do not consider the implications of the full high redshift cluster catalog here (cf. [11]).

If in the future a robust case can be made that a massive cluster falsifies both the ΛCDM and quintessence classes of models, then at least one cornerstone of modern cosmology must be incorrect: either the initial conditions are non-Gaussian, dark energy has non-canonical phantom behavior with $w < -1$, dark energy is not smooth even below the horizon, or dark energy interacts with the other components of the universe. The latter possibility includes both modified gravity scenarios and models where the scalar field responsible for the accelerating universe interacts with dark matter (e.g. [55–58]). Note that while changing the collisionless cold dark matter aspect of the cosmological paradigm can also change the cluster abundance, adding a massive neutrino component can only further suppress the cluster abundance.

Primordial non-Gaussianity, which typically skews the initial distribution of density fluctuations, can also in principle explain the existence of rare, massive, high redshift clusters [59]. For example, in the best-studied local model of primordial non-Gaussianity described by the parameter f_{NL} [60], positive f_{NL} would increase the number of clusters relative to $f_{\mathrm{NL}} = 0$ (e.g. [61]). However, to substantially change the abundance of high z clusters, a large positive value of f_{NL} (~ 400) seems to be required [10, 11, 62, 63], which, unless one resorts to postulating more complicated models with scale-dependent non-Gaussianity, is firmly ruled out by the combination of CMB [64, 65] and large scale structure [66–68] constraints.

Solutions involving dark energy also run into difficulties if the anomalous clusters appear only at high redshift. Typical solutions such as phantom (i.e. $w(z) < -1$ at any redshift) or clustered dark energy (e.g. [55, 69–71]) affect

cluster abundances at low redshift as much as or more than at high redshift given that the universe has only begun accelerating at $z \simeq 0.5$. The same is true of interacting dark energy or modified gravity scenarios where dark energy effectively mediates an enhanced attractive gravitational force (e.g. [72]). Thus models constructed to explain anomalous high redshift clusters while satisfying the CMB and expansion history constraints may still be ruled out by the local X-ray cluster sample [73, 74] or intermediate redshift samples (e.g. [75, 76]).

The standard cosmological paradigm has passed increasingly stringent tests over the last two decades. Current measurements of the expansion history are precise enough to make sharp predictions for cosmological structure formation. These predictions enable qualitatively new tests with which the standard paradigm and its extensions can be potentially falsified. Specifically, the masses of distant clusters must not be greater than a well-determined number set by the standard ΛCDM model if dark energy is a non-interacting canonical scalar field with equation of state $w \geq -1$, and if the initial conditions are Gaussian. Thus if increased survey coverage and improved cluster mass determination are found to strengthen claims of clusters that are substantially more massive or more distant than predicted in ΛCDM, then not only specific dark energy model incarnations but the whole quintessence paradigm would be falsified.

Appendix A: Fitting formulas

Here we provide a fitting formula to approximate the $M(z)$ exclusion curves of Fig. 4 and their dependence on the sky fraction and confidence levels for both sample and parameter variance. As an intermediate result, we also provide a fit to the median number of clusters expected above a given mass and redshift for flat ΛCDM, $\bar{N}_{P.50}(M, z)$ as well as its inverse $M(\bar{N}_{P.50}, z)$. These fits generalize the expressions provided in Ref. [5], which approximated $M(\bar{N}, z)$ for a single ΛCDM cosmology across a more limited range in masses and for disjoint sets of redshifts. We also give an approximate expression for the mass function logarithmic slope γ which can be used to estimate corrections for Eddington bias as described
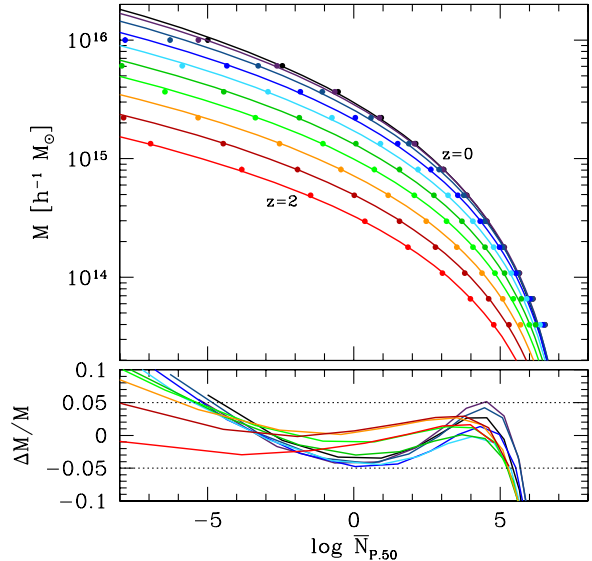

FIG. 7. Accuracy of our fitting formulas for $\bar{N}_{P.50}$, the median ΛCDM number of clusters in the whole sky above a given mass M and redshift z. *Upper panel:* numerical results from the MCMC analysis (points) compared with the approximate fitting formula of Eq. (A3) (curves). Several redshifts are shown, with equal spacing in $\ln(1+z)$ over $0 \leq z \leq 2$. *Lower panel:* fitting formula residuals. Dotted lines mark $\pm 5\%$ errors.

in § III C (see also Appendix C).

We begin by fitting an approximate formula for the median $\bar{N}_{P.50}(M, z)$ extracted from the flat ΛCDM posterior distributions. In order to ensure that the fitting function does not behave unphysically beyond the cases tested, we choose a functional form that is motivated by the mass function in Eqs. (7) and (8),

$$\bar{N}_{P.50} \propto e^{-C(M/M_*)^A}, \qquad (A1)$$

where A, C, and M_* are possibly redshift dependent quantities. This form follows by assuming that all terms in the mass function vary slowly with M except for the exponential, e^{-c/σ^2}, and that the dependence of $1/\sigma^2$ on M is well approximated by a power law. Hence we expect the fit to apply to rare objects such as clusters.

For notational simplicity let us define

$$m \equiv \log[M/(h^{-1} M_\odot)],$$
$$n \equiv \log \bar{N}_{P.50}. \qquad (A2)$$

Figure 7 shows that the following expressions are accurate to within 5% in mass over the ranges $14 < m < 16$, $0 < z < 2$, and $-5 < n < 5$:

$$n(m, z) = 7.65 \left[1 - e^{\alpha(z)(m - \beta(z))} \right], \qquad (A3)$$
$$\alpha(z) = 1.06 - 0.17 e^{-1.3z},$$
$$\beta(z) = 15.565 - 0.1 \log \left(7.1 + 10^{5.25z} \right).$$

In terms of the motivating form of Eq. (A1), $C = 7.65 \ln 10$, $A(z) = \alpha(z)/\ln 10$ and $M_*(z) =$

$10^{\beta(z)}\,h^{-1}\,M_\odot$. The approximate linearity of $\log M_*(z) \propto \beta(z)$ with z at high redshift was noted by Ref. [5] and indeed equating the scaling of M_* with a criterion like $\sigma(M_*) = $ const. implies that linearity extends to $z > 2$. This scaling is broken at low redshift mainly because the volume saturates and the number above a given z is determined not by the mass function around z but at a higher effective redshift.

Inverting Eq. (A3) gives the cluster mass as a function of redshift and n,

$$m(n, z) = \beta(z) + \frac{1}{\alpha(z)} \ln\left(1 - \frac{n}{7.65}\right), \qquad \text{(A4)}$$

where $\alpha(z)$ and $\beta(z)$ are the same as in Eq. (A3).

The above formulas apply to our predicted cluster abundances using MLCS2k2-fit SN data in addition to CMB, BAO, and H_0 constraints. The effective 10% shift in mass when using the SN data fit with the SALT2 method instead (see § III C) can be simply accounted for by replacing 15.565 with 15.525 in $\beta(z)$ in Eq. (A3):

$$\beta(z) = 15.525 - 0.1 \log\left(7.1 + 10^{5.25z}\right) \quad \text{(SALT2). (A5)}$$

With this change, the accuracy of the fitting formulas is the same regardless of the method used for fitting SN light curves.

The residuals increase at $n > 5$ independent of redshift since we only model the exponential part of the mass function where halos are rare. The fitting formulas agree with those of Ref. [5] to better than $\sim 10\%$ in mass for $-2 \le n \le 4$ while avoiding unphysical behavior at $n \le -2$.

These relations imply that the logarithmic slope of the mass function for the median ΛCDM model can be expressed in terms of $\log \bar N$ rather than M. Such a relation has the advantage that the logarithmic slope is a weak function of redshift at fixed number. Fitting to numerical results in Fig. 8 we obtain

$$\gamma(\bar N, z) = -\ln\left[2.6 + 1.5z^2 + e^{7.1 - 1.5 \exp(-3z) - 1.1 \log \bar N}\right]. \tag{A6}$$

Given the relationship between the median $\log \bar N = n$ and m in Eq. (A3), this expression gives the Eddington bias correction as a function of mass and redshift assuming the median ΛCDM predicted number. The fit to $\gamma(\bar N, z)$ is equally valid for predictions using both the MLCS2k2 and SALT2 SN analyses, although the relation between $\log \bar N$ and M differs as described above.

Changing the parameter variance exclusion level p changes the relationship between $\bar N$ and m (see Fig. 1). For a higher confidence level than the median $p = 0.5$ the predicted number at a fixed mass increases. Thus in order to find the mass m as a function of $\log \bar N$ for either exclusion curves or evaluating the logarithmic slope of the mass function, we need to shift the effective number density at which we evaluate Eqs. (A4) and (A6). We approximate $P(\log \bar N)$ as a lognormal distribution for the
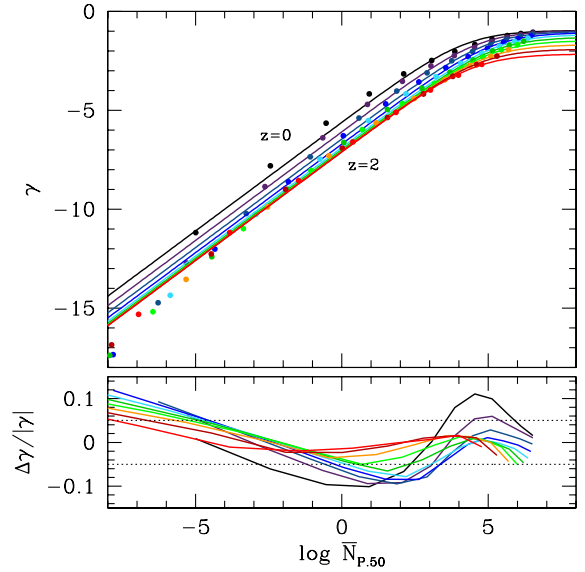

FIG. 8. Fit and residuals for the logarithmic slope of the mass function γ as a function of median cluster abundance and redshift. The fit uses the same points from the numerical calculation as in Fig. 7.

flat ΛCDM model class (see Fig. 1) with mean n and width

$$\sigma_{\log \bar N} = 0.29 - 0.035n, \tag{A7}$$

independent of redshift (fit to the distributions in Fig. 1 over $-8 < n < 6$). Then the relation between $\bar N$ and m and z at some parameter confidence p is given by

$$\log \bar N_{Pp}(m, z) = [1 - 0.035\sqrt{2}\,\mathrm{erf}^{-1}(2p - 1)]n(m, z)$$
$$+ 0.29\sqrt{2}\,\mathrm{erf}^{-1}(2p - 1). \tag{A8}$$

The inverse relationship between n and m of Eq. (A4),

$$\log \frac{M(z; s, p, f_{\mathrm{sky}})}{h^{-1}\,M_\odot} = m(n(s, p, f_{\mathrm{sky}}), z), \tag{A9}$$

can then be evaluated at

$$n = \frac{\log(-f_{\mathrm{sky}}^{-1}\ln s) - 0.29\sqrt{2}\,\mathrm{erf}^{-1}(2p - 1)}{1 - 0.035\sqrt{2}\,\mathrm{erf}^{-1}(2p - 1)}, \tag{A10}$$

which comes from Eq. (A8) using the criterion that the $100s\%$ CL sets $\bar N_{Pp} = \bar N_{Ss} = -f_{\mathrm{sky}}^{-1}\ln s$. Equation (A9) therefore gives the desired exclusion curves at a given sample variance CL, parameter variance CL, and sky fraction. The Eddington bias at a given parameter variance confidence, mass, and redshift can also be evaluated by using Eqs. (A8) and (A3) in Eq. (A6).

These formulas also provide a convenient way to estimate the significance of an observed cluster: given the cluster mass and redshift, Eq. (A3) approximates the median expected cluster abundance in the full sky, and
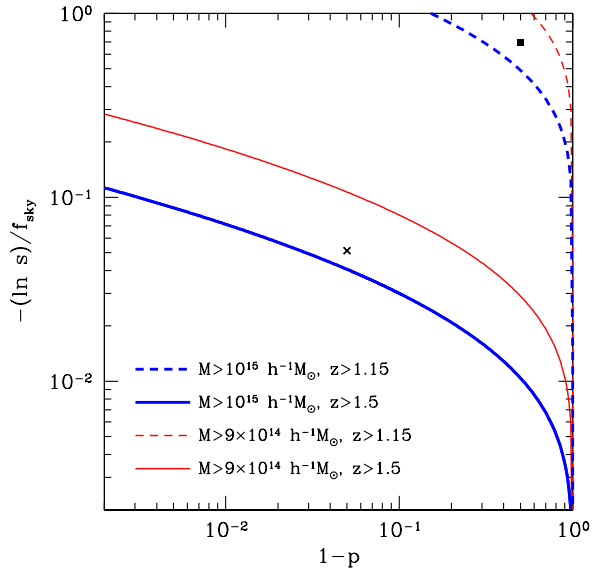
FIG. 9. Combinations of $100s\%$ CL and $100p\%$ CL limits for sample variance and parameter variance, respectively, given various mass and redshift thresholds. In the limit of high significance for sample variance ($1 - s \ll 1$), $-f_{\mathrm{sky}}^{-1} \ln s \approx f_{\mathrm{sky}}^{-1}(1 - s)$. The curves are computed using the fitting formulas of Eqs. (A3) and (A10). The 95% joint CL values used in § III A and the 50% joint CL values for $f_{\mathrm{sky}} = 1$ are marked with a cross and a square, respectively.
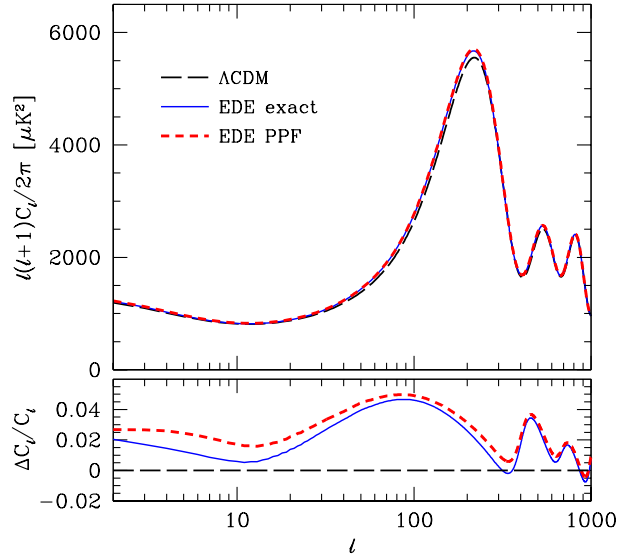
FIG. 10. CMB temperature power spectrum of an EDE model calculated exactly from the scalar field equations and in the PPF approximation, compared with a ΛCDM model with the same matter density, baryon density, distance to last scattering, and initial curvature power spectrum. The transition from clustered to smooth EDE boosts the CMB power spectrum around the first peak, and thus matching the WMAP7 normalization requires small changes in A_s and n_s from their ΛCDM values.

Eq. (A10) then determines the corresponding combinations of sample variance and parameter variance confidence limits for flat ΛCDM. Note in particular that $-f_{\mathrm{sky}}^{-1} \ln[s(m, z; p)]$ can be extracted as a closed form expression. Figure 9 shows examples of these s–p relations for clusters with $M \approx 10^{15}\, h^{-1}\, M_\odot$ at redshifts $z = 1.15$ and 1.5, for which the significance of excluding flat ΛCDM is near the 50% joint CL and 95% joint CL, respectively. For high significance clusters, a 10% change in mass shifts the exclusion curves by a factor of a few in $(1 - s)/f_{\mathrm{sky}}$ and over an order of magnitude in $(1 - p)$, highlighting again the importance of accurate mass determination.

Appendix B: Normalization and Early Dark Energy

High redshift cluster abundance constraints are often phrased relative to the local cluster abundance by fixing σ_8 and Ω_{m}. Despite how well these two parameters are constrained in flat ΛCDM by the WMAP7 data, this is not equivalent to normalizing to CMB data.

In particular, the assumption that the value of σ_8 is well known requires extrapolating from the measurement at $z_* = 1090$ to the present using a particular growth function, and in general changing the dark energy model results in a different growth function implying a different value of σ_8 for fixed CMB amplitude. Additionally, the presence of EDE directly affects CMB fluctuations

on the horizon scale at recombination due to its transition from an adiabatically clustered to relatively smooth component.

Our normalization parameter is A_s, the amplitude of the *initial* curvature power spectrum at $k = 0.05\, \mathrm{Mpc}^{-1}$, and we use the CAMB PPF module to propagate its effects jointly with the effects of EDE on the observable CMB power spectra. The PPF approximation retains the quintessence property that the sound speed of dark energy is equal to the speed of light but implements the transition from a clustered to smooth component in an approximate manner [29].

In Fig. 10 we compare a ΛCDM model and a quintessence model with EDE which have the same A_s, n_s, $\Omega_{\mathrm{c}}h^2$, $\Omega_{\mathrm{b}}h^2$ and $D(z_*)$. Specifically, we choose an offset exponential for the quintessence potential

$$V(\phi) = V_0 + A \exp(-\phi/\phi_*). \qquad \text{(B1)}$$

For this potential, quintessence behaves as a tracking field at early times with $w \approx 0$ during matter domination, and as a cosmological constant at late times. We first calculate the exact CMB power spectrum for this model and then compare it with the PPF approximation. The EDE to matter ratio at z_* is determined by ϕ_* (e.g. [77]) and we have chosen it to correspond to 3.3% while the ratio of EDE to the total density is 2.4%. The potential offset V_0 is set by demanding that $D(z_*)$ remain fixed in a flat universe, and A is set by requiring that the field be in the tracking regime well before recombination.
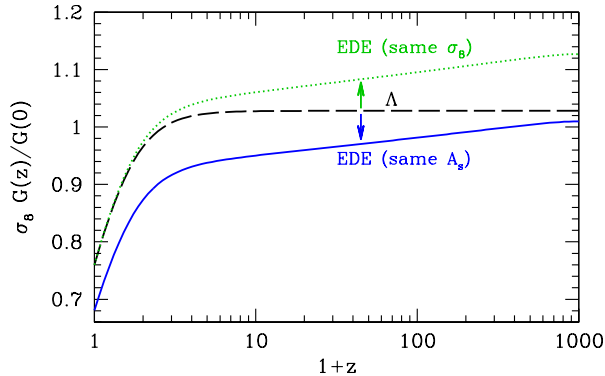
FIG. 11. Illustration of the varying effects of early dark energy depending on whether the growth history is normalized at $z = 0$ by fixing σ_8 or at $z \sim 10^3$ by fixing A_s. The ΛCDM and EDE example models from Fig. 10 are shown by the dashed black and solid blue curves, respectively; the dotted green curve shows the same EDE model with σ_8 rescaled to match its value in the ΛCDM model.

Note that to zeroth order the CMB power at the $\ell \sim 200$ first peak remains largely fixed given the same initial curvature power spectrum, but the small EDE fraction causes a first order correction. The decay of gravitational potentials due to the EDE becoming smooth under the horizon scale leads to a small boost in the amplitude. Conversely, at fixed WMAP7 normalization, the best fit A_s is slightly reduced, while the best fit n_s increases to preserve the amplitude of the first peak where the EDE is most effective ($k \approx 0.02\,\mathrm{Mpc}^{-1}$ compared with our pivot scale of $0.05\,\mathrm{Mpc}^{-1}$). Moreover, the boost widens the first peak and since this effect is not degenerate with changes in A_s and n_s or other cosmological parameters, it provides limits on EDE from the CMB alone [78]. The PPF approximation captures these effects to sufficient accuracy for models that satisfy these observational bounds.

We obtain σ_8 and more generally $\sigma(M, z = 0)$ for each cosmological model using the PPF version of CAMB. Even the small EDE fraction of our example can have a sizable effect on $\sigma(M, z = 0)$ due to the long lever arm between z_* and $z = 0$ over which the change in the subhorizon growth rate can act. To obtain $\sigma(M, z)$ at $z > 0$, we compute $G(z)$ by integrating the differential equation for the linear growth function as described in [13]. Since we use the growth function only to scale backwards from the present epoch, all high redshift modifications to the transfer function and the CMB normalization of $\sigma(M, 0)$ through A_s are accounted for, including the impact of the EDE clustering transition. This procedure is illustrated in Fig. 11 (lowest curve). We then assume that $\sigma(M, z)$ determines the halo mass function with no explicit dependence on EDE. Note that this differs from [49, 50] who took a spherical collapse motivated mass function with a collapse threshold δ_c that depended on EDE. The modified threshold ansatz was later shown to be inconsistent with both numerical and analytic results [51–54].

The alternate approach of assuming a fixed value of σ_8 leads to very different conclusions about the effects of EDE. In that case, the similar shapes of the ΛCDM and EDE growth functions at low redshifts imply that the effects of EDE on cluster abundances are small (upper curves in Fig. 11 at low z) [51–54]. However, Fig. 11 combined with Fig. 10 shows that a model with a substantial amount of EDE and σ_8 fixed to the best fit ΛCDM value would change the high redshift normalization A_s and hence the CMB power spectrum normalization. In this example, the shift is more than 10% in amplitude, whereas the CMB normalization for a given A_s is determined to an accuracy of $\sim 1.4\%$ corresponding to the uncertainty in the reionization optical depth. Conversely, by requiring consistency with the CMB, the effect of EDE on *reducing* the cluster abundance can be quite large as shown in Fig. 3 (see also [79, 80]).

Appendix C: Eddington Bias

For a steep mass function, an observable proxy for cluster mass M_obs is biased high compared with the true mass M since it is more likely that one of the numerous low mass objects scatters to higher M_obs than it is that a rare high mass object scatters to lower M_obs. There are two types of mass bias associated with this effect and we clarify their use here.

Consider first the type relevant to the exclusion analysis of the main part of the paper. We seek to find the probability of a given model producing a cluster with observed mass greater than M_obs at the given redshift or above. The generalization of $\bar{N}$, the number of clusters above a given true mass and redshift, is

$$\bar{N}_\mathrm{obs}(M_\mathrm{obs}, z) = \int_z^\infty dz' \frac{4\pi D^2(z')}{H(z')} \int_{M_\mathrm{obs}}^\infty \frac{dM'_\mathrm{obs}}{M'_\mathrm{obs}} \int_0^\infty \frac{dM'}{M'}$$
$$\times \frac{dn}{d\ln M}(M', z') P(\ln M'_\mathrm{obs}|\ln M'), \quad \text{(C1)}$$

where $P(\ln M_\mathrm{obs}|\ln M)$ is the probability density of obtaining an observed mass M_obs given a true mass M. In order to set the probability of finding a cluster of observed mass $> M_\mathrm{obs}$ equal to finding a cluster of true mass $> M$ we require

$$\bar{N}_\mathrm{obs}(M_\mathrm{obs}, z) = \bar{N}(M_N, z). \quad \text{(C2)}$$

The difference between M_N and M_obs is the *number bias* mass shift. By setting the probabilities equal, we therefore have the same exclusion confidence as if we had measured a cluster with true mass M_N.

For the case of a lognormal mass observable relation with rms $\sigma_{\ln M}$ that is small compared with the scale over which the local slope of the mass function changes, $dn/d\ln M \propto M^\gamma$ and [44, 45]

$$\ln M_N = \ln M_\mathrm{obs} + \frac{1}{2}\gamma\sigma_{\ln M}^2. \quad \text{(C3)}$$

This is the appropriate mass to plot on an $M(z)$ exclusion plot. Note that $\gamma < 0$ so $M_N < M_{\rm obs}$.

There is a second sense of a bias in mass that is commonly used in the literature. To place confidence limits on the mass assuming a mass function and an observed mass $M_{\rm obs}$, one can use Bayes' theorem [81, 82]

$$P(\ln M \,|\, \ln M_{\rm obs}) \propto P(\ln M) P(\ln M_{\rm obs} \,|\, \ln M) \qquad (\text{C4})$$

and take $P(\ln M) \propto dn/d\ln M$. For the same lognormal and constant slope assumptions, the posterior mass distribution is a lognormal of the same width $\sigma_{\ln M}$ and

shifted mean

$$\ln M_M = \ln M_{\rm obs} + \gamma \sigma_{\ln M}^2 \,, \qquad (\text{C5})$$

which is twice the mass shift required to hold probabilities fixed. Note that this *mass bias* mass shift is the answer to a statistically different question. Here one assumes that the observation is fixed and the mass function is *a priori* correct. One does not account for the probability of drawing such an $M_{\rm obs}$ (or greater) from the mass function and the mass observable relation. In other words, Eq. (C5) is the appropriate correction for quoting confidence levels for the mass assuming ΛCDM, and Eq. (C3) is the appropriate correction for quoting confidence levels for how the existence of a given cluster might exclude ΛCDM. It is the latter that we are interested in here.

[1] N. A. Bahcall and X.-h. Fan, Astrophys. J., **504**, 1 (1998), arXiv:astro-ph/9803277.
[2] Z. Haiman, J. J. Mohr, and G. P. Holder, Astrophys. J., **553**, 545 (2001), arXiv:astro-ph/0002336.
[3] J. Weller, R. Battye, and R. Kneissl, Phys. Rev. Lett., **88**, 231301 (2002), arXiv:astro-ph/0110353.
[4] M. Oguri and R. D. Blandford, Mon. Not. Roy. Astron. Soc., **392**, 930 (2009), arXiv:0808.0192.
[5] D. E. Holz and S. Perlmutter, (2010), arXiv:1004.5349.
[6] C. R. Mullis *et al.*, Astrophys. J., **623**, L85 (2005), arXiv:astro-ph/0503004.
[7] M. Lombardi *et al.*, Astrophys. J., **623**, 42 (2005), arXiv:astro-ph/0501150.
[8] M. Brodwin *et al.*, Astrophys. J., **721**, 90 (2010), arXiv:1006.5639.
[9] M. J. Jee *et al.*, Astrophys. J., **704**, 672 (2009), arXiv:0908.3897.
[10] L. Cayon, C. Gordon, and J. Silk, (2010), arXiv:1006.1950.
[11] B. Hoyle, R. Jimenez, and L. Verde, (2010), arXiv:1009.3884.
[12] M. J. Mortonson, W. Hu, and D. Huterer, Phys. Rev., **D81**, 063007 (2010), arXiv:0912.3816.
[13] M. J. Mortonson, W. Hu, and D. Huterer, Phys. Rev., **D79**, 023004 (2009), arXiv:0810.1744.
[14] R. Kessler *et al.*, Astrophys. J. Suppl., **185**, 32 (2009), arXiv:0908.4274.
[15] W. M. Wood-Vasey *et al.*, Astrophys. J., **666**, 694 (2007), arXiv:astro-ph/0701041.
[16] P. Astier *et al.*, Astron. Astrophys., **447**, 31 (2006), arXiv:astro-ph/0510447.
[17] A. G. Riess *et al.*, Astrophys. J., **659**, 98 (2007), arXiv:astro-ph/0611572.
[18] S. Jha, A. G. Riess, and R. P. Kirshner, Astrophys. J., **659**, 122 (2007), arXiv:astro-ph/0612666.
[19] J. Guy *et al.*, Astron. Astrophys., **466**, 11 (2007), arXiv:astro-ph/0701828.
[20] R. Amanullah *et al.*, Astrophys. J., **716**, 712 (2010), arXiv:1004.1711.
[21] M. Hicken *et al.*, Astrophys. J., **700**, 1097 (2009), arXiv:0901.4804.

[22] M. Kowalski *et al.*, Astrophys. J., **686**, 749 (2008), arXiv:0804.4142.
[23] D. Larson *et al.*, (2010), arXiv:1001.4635.
[24] http://lambda.gsfc.nasa.gov/.
[25] C. Dvorkin and W. Hu, Phys. Rev., **D82**, 043513 (2010), arXiv:1007.0215.
[26] http://background.uchicago.edu/wmap_fast.
[27] A. Lewis, A. Challinor, and A. Lasenby, Astrophys. J., **538**, 473 (2000), arXiv:astro-ph/9911177.
[28] http://camb.info/.
[29] W. Fang, W. Hu, and A. Lewis, Phys. Rev., **D78**, 087303 (2008), arXiv:0808.3125.
[30] http://camb.info/ppf/.
[31] W. J. Percival, S. Cole, D. J. Eisenstein, R. C. Nichol, J. A. Peacock, A. C. Pope, and A. S. Szalay, Mon. Not. Roy. Astron. Soc., **381**, 1053 (2007), arXiv:0705.3323.
[32] A. G. Riess *et al.*, Astrophys. J., **699**, 539 (2009), arXiv:0905.0695.
[33] A. Lewis and S. Bridle, Phys. Rev., **D66**, 103511 (2002), arXiv:astro-ph/0205436.
[34] http://cosmologist.info/cosmomc/.
[35] A. Gelman and D. Rubin, Statistical Science, **7**, 457 (1992).
[36] M. Mortonson, W. Hu, and D. Huterer, Phys. Rev., **D80**, 067301 (2009), arXiv:0908.1408.
[37] J. L. Tinker *et al.*, Astrophys. J., **688**, 709 (2008), arXiv:0803.2706.
[38] S. Bhattacharya *et al.*, (2010), arXiv:1005.2239.
[39] W. Hu and A. V. Kravtsov, Astrophys. J., **584**, 702 (2003), arXiv:astro-ph/0203169.
[40] K. Andersson *et al.*, (2010), arXiv:1006.3068.
[41] J. P. Stott *et al.*, Astrophys. J., **718**, 23 (2010), arXiv:1005.4681.
[42] T. A. Marriage *et al.*, (2010), arXiv:1010.1065.
[43] A. Eddington, Mon. Not. Roy. Astron. Soc., **73**, 350 (1913).
[44] M. Lima and W. Hu, Phys. Rev., **D72**, 043006 (2005), arXiv:astro-ph/0503363.
[45] R. Stanek, A. E. Evrard, H. B. Bohringer, P. Schuecker, and B. Nord, Astrophys. J., **648**, 956 (2006), arXiv:astro-

ph/0602324.

[46] Z. Lukic, D. Reed, S. Habib, and K. Heitmann, Astrophys. J., **692**, 217 (2009), arXiv:0803.3624.

[47] A. Jenkins, C. Frenk, S. D. White, J. Colberg, S. Cole, *et al.*, Mon.Not.Roy.Astron.Soc., **321**, 372 (2001), arXiv:astro-ph/0005260.

[48] R. J. Foley *et al.*, (2010), arXiv:1010.2749.

[49] M. Bartelmann, M. Doran, and C. Wetterich, Astron. Astrophys., **454**, 27 (2006), arXiv:astro-ph/0507257.

[50] S. Sadeh, Y. Rephaeli, and J. Silk, Mon. Not. Roy. Astron. Soc., **380**, 637 (2007), arXiv:0706.1340.

[51] M. J. Francis, G. F. Lewis, and E. V. Linder, Mon. Not. Roy. Astron. Soc., **394**, 605 (2008), arXiv:0808.2840.

[52] M. Grossi and V. Springel, Mon. Not. Roy. Astron. Soc., **394**, 1559 (2009), arXiv:0809.3404.

[53] M. J. Francis, G. F. Lewis, and E. V. Linder, Mon. Not. Roy. Astron. Soc. Lett., **393**, L31 (2008), arXiv:0810.0039.

[54] F. Pace, J. Waizmann, and M. Bartelmann, Mon. Not. Roy. Astron. Soc., **406**, 1865 (2010), arXiv:1005.0233.

[55] M. Manera and D. F. Mota, Mon. Not. Roy. Astron. Soc., **371**, 1373 (2006), arXiv:astro-ph/0504519.

[56] S. Das, P. S. Corasaniti, and J. Khoury, Phys. Rev., **D73**, 083509 (2006), arXiv:astro-ph/0510628.

[57] E. Abdalla, L. R. W. Abramo, L. Sodre, Jr., and B. Wang, Phys. Lett., **B673**, 107 (2009), arXiv:0710.1198.

[58] M. Baldi and V. Pettorino, (2010), arXiv:1006.3761.

[59] W. A. Chiu, J. P. Ostriker, and M. A. Strauss, Astrophys. J., **494**, 479 (1998), arXiv:astro-ph/9708250.

[60] E. Komatsu and D. N. Spergel, Phys. Rev., **D63**, 063002 (2001), arXiv:astro-ph/0005036.

[61] E. Sefusatti, C. Vale, K. Kadota, and J. Frieman, Astrophys. J., **658**, 669 (2007), arXiv:astro-ph/0609124.

[62] R. Jimenez and L. Verde, Phys. Rev., **D80**, 127302 (2009), arXiv:0909.0403.

[63] B. Sartoris, S. Borgani, C. Fedeli, S. Matarrese, L. Moscardini, P. Rosati, and J. Weller, Mon. Not. Roy. Astron. Soc., **407**, 2339 (2010), arXiv:1003.0841.

[64] E. Komatsu *et al.*, (2010), arXiv:1001.4538.

[65] K. M. Smith, L. Senatore, and M. Zaldarriaga, JCAP, **0909**, 006 (2009), arXiv:0901.2572.

[66] A. Slosar, C. Hirata, U. Seljak, S. Ho, and N. Padmanabhan, JCAP, **0808**, 031 (2008), arXiv:0805.3580.

[67] N. Afshordi and A. J. Tolley, Phys. Rev., **D78**, 123507 (2008), arXiv:0806.1046.

[68] F. De Bernardis, P. Serra, A. Cooray, and A. Melchiorri, Phys. Rev., **D82**, 083511 (2010), arXiv:1004.5467.

[69] N. J. Nunes, A. C. da Silva, and N. Aghanim, Astron. Astrophys., **450**, 899 (2006), arXiv:astro-ph/0506043.

[70] L. R. Abramo, R. C. Batista, and R. Rosenfeld, JCAP, **0907**, 040 (2009), arXiv:0902.3226.

[71] P. Creminelli, G. D'Amico, J. Norena, L. Senatore, and F. Vernizzi, JCAP, **1003**, 027 (2010), arXiv:0911.2701.

[72] F. Schmidt, M. V. Lima, H. Oyaizu, and W. Hu, Phys. Rev., **D79**, 083518 (2009), arXiv:0812.0545.

[73] H. Ebeling, A. Edge, S. Allen, C. Crawford, A. Fabian, *et al.*, Mon.Not.Roy.Astron.Soc., **318**, 333 (2000), arXiv:astro-ph/0003191.

[74] H. Boehringer *et al.*, Astron. Astrophys., **425**, 367 (2004), arXiv:astro-ph/0405546.

[75] E. Rozo *et al.*, Astrophys. J., **708**, 645 (2010), arXiv:0902.3702.

[76] A. Vikhlinin *et al.*, Astrophys. J., **692**, 1033 (2009), arXiv:0805.2207.

[77] P. G. Ferreira and M. Joyce, Phys.Rev., **D58**, 023503 (1998), arXiv:astro-ph/9711102.

[78] M. Doran and G. Robbers, JCAP, **0606**, 026 (2006), arXiv:astro-ph/0601544.

[79] U. Alam, Z. Lukic, and S. Bhattacharya, (2010), arXiv:1004.0437.

[80] S. Basilakos, M. Plionis, and J. A. S. Lima, Phys. Rev., **D82**, 083517 (2010), arXiv:1006.3418.

[81] D. W. Hogg and E. L. Turner, Publ. Astron. Soc. Pac., **110**, 727 (1998), arXiv:astro-ph/9711154.

[82] K. Vanderlinde *et al.*, Astrophys. J., **722**, 1180 (2010), arXiv:1003.0003.